

19. Cristobal, S., Scotti, P., Luirink, J., von Heijne, G. & de Gier, J.-W. L. The signal recognition particle-targeting pathway does not necessarily deliver proteins to the Sec-translocase in *Escherichia coli*. *J. Biol. Chem.* **274**, 20068–20070 (1999).

20. Gilmore, R., Collins, P., Johnson, J., Kellaris, K. & Rapiejko, P. Transcription of full-length and truncated mRNA transcripts to study protein translocation across the endoplasmic reticulum. *Methods Cell Biol.* **34**, 223–237 (1991).

21. Martoglio, B., Hofmann, M. W., Brunner, J. & Dobberstein, B. The protein-conducting channel in the membrane of the endoplasmic reticulum is open laterally toward the lipid bilayer. *Cell* **18**, 207–214 (1995).

22. Scotti, P. A. *et al.* YidC, the *Escherichia coli* homologue of mitochondrial Oxa1p, is a component of the Sec translocase. *EMBO J.* **19**, 542–549 (2000).

23. Görlich, D., Hartmann, E., Prehn, S. & Rapoport, T. A. A protein of the endoplasmic reticulum involved early in polypeptide translocation. *Nature* **357**, 47–52 (1992).

24. Do, H., Falcone, D., Lin, J., Andrews, D. W. & Johnson, A. E. The cotranslational integration of membrane proteins into the phospholipid bilayer is a multistep process. *Cell* **85**, 369–378 (1996).

25. Platt, R., Drescher, C. D., Park, S. K. & Phillips, G. J. Genetic system for reversible integration of DNA constructs and *lacZ* gene fusions into the *Escherichia coli* chromosome. *Plasmid* **43**, 12–23 (2000).

26. Hamilton, C. M., Aldea, M., Washburn, B. K., Babbitzke, P. & Kushner, S. R. New method for generating deletions and gene replacements in *Escherichia coli*. *J. Bacteriol.* **171**, 4617–4622 (1989).

27. Graf, R., Brunner, J., Dobberstein, B. & Martoglio, B. in *Cell Biology: a Laboratory Handbook* 2nd edn, Vol. 4, (ed. Celis, J. E.) 495–501 (Academic, San Diego, 1998).

28. Brunner, J. Use of photocrosslinkers in cell biology. *Trends Cell Biol.* **6**, 154–157 (1996).

29. Cload, S. T., Liu, D. R., Froland, W. A. & Schultz, P. Development of improved tRNAs for *in vitro* biosynthesis of proteins containing unnatural amino acids. *Chem. Biol.* **3**, 1033–1038 (1996).

30. Gold, L. M. & Schweiger, M. in *Methods in Enzymology* Vol. 20, (eds Moldave, K. & Grossman, L.) 537–542 (Academic, London and New York, 1971).

Acknowledgements

We thank P. G. Schultz for the *E. coli* suppressor tRNA^{Asn} gene, S. R. Kushner for knockout vector pMAK705, J.-W. de Gier for the ProW construct, J. Brunner for the photocrosslinking reagent (Tmd)Phe-pdCpA, and Matthias Muller for advice with the amber suppression studies. This work was supported by an NSF grant (to R.E.D.) and by a DFG grant (to A.K.).

Correspondence and requests for materials should be addressed to R.E.D. (e-mail: dalbey@chemistry.ohio-state.edu).

Telomere dysfunction promotes non-reciprocal translocations and epithelial cancers in mice

Steven E. Artandi*, Sandy Chang††, Shwu-Luan Lee*, Scott Alison*, Geoffrey J. Gottlieb‡§, Lynda Chin*|| & Ronald A. DePinho*¶

* Department of Adult Oncology, Dana-Farber Cancer Institute, Boston, Massachusetts 02115, USA
 † Department of Pathology, Brigham and Women's Hospital, Boston, Massachusetts 02115, USA
 ‡ CPI Ameripath Laboratory, Beachwood, Ohio 44122, USA
 § Ackerman Academy of Dermatopathology, New York, New York 10016, USA
 || Department of Dermatology, Harvard Medical School, Boston, Massachusetts 02115, USA
 ¶ Departments of Genetics and Medicine, Harvard Medical School, Boston, Massachusetts 02115, USA

Aged humans sustain a high rate of epithelial cancers such as carcinomas of the breast and colon, whereas mice carrying common tumour suppressor gene mutations typically develop soft tissue sarcomas and lymphomas. Among the many factors that may contribute to this species variance are differences in telomere length and regulation. Telomeres comprise the nucleoprotein complexes that cap the ends of eukaryotic chromosomes and are maintained by the reverse transcriptase, telomerase¹. In human cells, insufficient levels of telomerase lead to telomere attrition with cell division in culture² and possibly with ageing and tumorigenesis *in vivo*^{3–5}. In contrast, critical reduction in telomere length is not observed in the mouse owing to promiscuous telomerase expression and long telomeres^{6–10}. Here we

provide evidence that telomere attrition in ageing telomerase-deficient p53 mutant mice promotes the development of epithelial cancers by a process of fusion-bridge breakage that leads to the formation of complex non-reciprocal translocations—a classical cytogenetic feature of human carcinomas. Our data suggest a model in which telomere dysfunction brought about by continual epithelial renewal during life generates the massive ploidy changes associated with the development of epithelial cancers.

Chromosomal rearrangement mechanisms are intimately linked to cancer development and are thought to generate the numerous gains and losses of segments of chromosomes needed for epithelial carcinogenesis. These wholesale and complex rearrangements typically occur early, by the carcinoma-*in-situ* stage, but appear to be largely unchanged with progression to invasive and metastatic disease^{11–13}. Additional genomic alterations and mutations no doubt accrue during tumour progression, but these data suggest that the instability of cancer genomes is episodic, primarily occurring early during carcinogenesis and resolving to relative stability in advanced malignancy. These genomic changes are evident by the stage when telomerase is first activated^{14,15}, which suggests that an early and transient period of telomere dysfunction could contribute to complex genomic alterations encountered in mature epithelial cancers.

Mice lacking the RNA component of telomerase (mTERC) exhibit progressive telomere shortening and ultimately chromosomal instability (end-to-end fusions) as a function of age and of successive generational matings^{16,17}. Paradoxically, although telomerase facilitates oncogenic transformation of cultured human cells¹⁸, telomere shortening in ageing mTERC^{-/-} mice is associated with increased rates of cancer, suggesting that the genetic instability

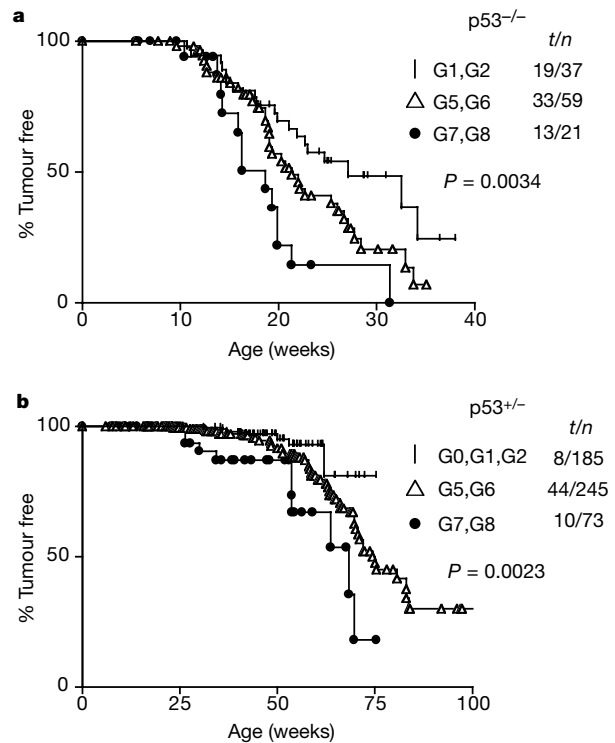


Figure 1 Kaplan–Meier analysis of tumour incidence in p53 mutant mice divided on the basis of generation of telomerase deficiency. **a**, p53^{-/-} mice. The number of tumours identified (*t*) and the total number of mice (*n*) in each cohort is indicated. Hatched line, G1–G2 mTERC^{-/-}; triangles, G5–G6 mTERC^{-/-}; circles, G7–G8 mTERC^{-/-}. **b**, p53^{+/-} mice. Hatched line, mTERC^{+/-}, mTERC^{+/-} or G1–G2 mTERC^{-/-}; triangles, G5–G6 mTERC^{-/-}; circles, G7–G8 mTERC^{-/-}.

Table 1 Histological diagnoses of spontaneous tumours

| Histological type | Telomere function intact | | Telomere dysfunction | |
|---|--------------------------|--------------|----------------------|--------------|
| | No. | % of tumours | No. | % of tumours |
| Tumour spectrum in p53^{-/-} mice | | | | |
| Thymic lymphoma | 23 | 64 | 24 | 54 |
| Other lymphoma | 3 | 8 | 2 | 4 |
| Sarcoma | 9 | 25 | 15 | 33 |
| Glioma, spinal cord | 1 | 3 | 0 | 0 |
| Adenocarcinoma | 0 | 0 | 4 | 9 |
| Total | 36 | | 100 | 45 |
| Tumour spectrum in p53^{+/-} mice* | | | | |
| Breast adenocarcinoma | 0 | 0 | 10 | 10 |
| Squamous cell carcinoma | 0 | 0 | 21 | 22 |
| Gastrointestinal adenocarcinoma | 0 | 0 | 19 | 20 |
| Other carcinoma | 0 | 0 | 3 | 3 |
| Osteosarcoma | 2 | 25 | 17 | 18 |
| Angiosarcoma | 0 | 0 | 4 | 4 |
| Other sarcoma | 4 | 50 | 11 | 11 |
| Ovarian stromal cell tumour | 0 | 0 | 4 | 4 |
| Lymphoma | 2 | 25 | 8 | 8 |
| Total | 8 | 100 | 97 | 100 |

*p53^{-/-} mice were compared between two cohorts: one with intact telomeres (mTERC^{+/+}, mTERC^{+/-}, G1–G2 mTERC^{-/-}) and one with severe telomere dysfunction (G5–G8 mTERC^{-/-}).

associated with telomere dysfunction can facilitate transformation *in vivo*¹⁹. Moreover, loss of p53 improves the survival of cells with telomere dysfunction, and thus has a permissive role in the generation of end-to-end chromosomal fusions and aneuploidy. In the setting of p53 deficiency, telomere dysfunction confers a greater susceptibility to transformation by cellular oncogenes²⁰. Despite these observations, the precise mechanism by which telomere

dysfunction facilitates cancer and the implications of these tissue culture experiments for tumorigenesis *in vivo* remained unclear.

Although telomerase is reactivated in most mature human cancers, we sought to model the early stages of tumorigenesis in which telomere shortening and dysfunction might impair chromosomal integrity. We monitored the cancer phenotype and cytogenetics of large cohorts of telomerase-deficient p53 mutant mice. In generation one (G1) and generation two (G2) mTERC^{-/-} p53^{-/-} mice that lack telomerase but retain normal telomere function, median tumour incidence was similar to that of mTERC^{+/+} p53^{-/-} and mTERC^{+/-} p53^{-/-} controls (27.1 compared with 24.9 weeks, $P = 0.212$; data not shown). In contrast, in later mTERC^{-/-} generations the progressive decline in telomere function correlated with decreasing tumour latency: 27.1 weeks for G1–G2, 21.3 weeks for G5–G6, and 18.6 weeks for G7–G8 mTERC^{-/-} p53^{-/-} cohorts ($P = 0.0034$; Fig. 1a). Similarly, in p53^{+/-} cohorts median tumour latency decreased progressively as telomeres became short and dysfunctional ($P = 0.0023$; Fig. 1b). Seven out of nine tumours of late generation mTERC^{-/-} p53^{+/-} mice exhibited loss of the remaining p53 wild-type allele (data not shown). Thus, telomere dysfunction, rather than loss of telomerase *per se*, cooperates with p53 deficiency to accelerate tumorigenesis *in vivo*, in agreement with previous transformation studies in cell culture²⁰.

Sarcomas and lymphomas dominated the tumour spectrum of late generation mTERC^{-/-} p53^{-/-} mice (Table 1), similar to previous reports of p53^{-/-} mice^{21,22}. However, the emergence of adenocarcinomas in late generation mTERC^{-/-} p53^{-/-} mice (9%), compared with none in early generation controls, suggested that telomere dysfunction may be involved in promoting epithelial carcinogenesis. Because p53^{-/-} mice succumb rapidly to lymphoid and mesenchymal cancers, we reasoned that the much longer tumour latency of p53^{+/-} mice^{21,22} might reveal an impact of age-dependent

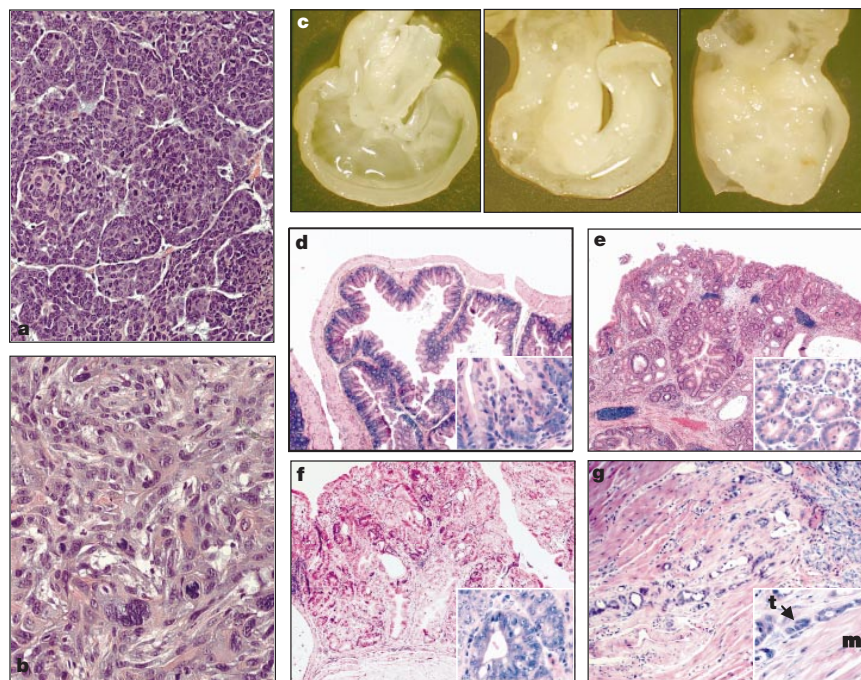


Figure 2 Histology of epithelial cancers in mice with telomere dysfunction. **a**, Breast cancer, G5 mTERC^{-/-} p53^{+/-} mouse; **b**, squamous cell carcinoma, G6 mTERC^{-/-} p53^{+/-} mouse. H&E stain, original magnification $\times 20$. **c**, Gross view of caeca from mTERC^{+/+} p53^{+/-} (left), G6 mTERC^{-/-} p53^{+/-} (middle), and G5 mTERC^{-/-} p53^{+/-} (right). **d**, Histology of normal caecum, mTERC^{+/+} p53^{+/-}, shows typical colonic villi and ordered nuclei. H&E stain, original magnification $\times 4$; inset, $\times 20$. **e**, Adenomatous polyp in the caecum, G5

mTERC^{-/-} p53^{+/-}. Inset, glands remain round with basal nuclei. H&E stain, original magnification $\times 4$; inset, $\times 20$. **f**, Caecal adenocarcinoma, G5 mTERC^{-/-} p53^{+/-}. Inset, disordered glands and pleiomorphic nuclei. Original magnification $\times 4$; inset $\times 20$. **g**, Invasive adenocarcinoma of colon, G5 mTERC^{-/-} p53^{+/-}. Inset, tumour cells (t) with poor glandular organization invading muscle fibres (m). H&E stain, original magnification $\times 10$; inset, $\times 20$.

telomere attrition on tumorigenesis in self-renewing epithelial compartments. We subjected 97 tumours arising in 81 late generation $mTERC^{-/-}$ $p53^{+/-}$ mice to detailed histological and tumour marker analysis (Table 1). Carcinomas represented the largest class of clinically apparent tumours (55%, but occult carcinomas occurred in all mice, see below), exceeding sarcomas (37%) and lymphomas (8%).

Adenocarcinoma of the breast presented as solitary subcutaneous masses along the milk line in female mice only, and, on the histological level, showed carcinoma cells growing in nested patterns (Fig. 2a). Squamous cell carcinomas of the skin showed characteristic morphology (keratin pearls and intercellular bridges, Fig. 2b), and immunoreactivity to cytokeratins—markers commonly used to diagnose human epithelial cancers (see Supplementary Information). A subset of mice ($n = 16$) exhibited either distension of the gastrointestinal tract or caecal enlargement. In roughly 75% of these mice, gross examination of the caecum revealed a macroscopic polyp, usually extending along the luminal wall of the caecum without a discernible stalk (sessile polyp), findings typical of caecal polyps in humans (Fig. 2c). Histologically, these lesions showed a spectrum of abnormalities from adenomatous proliferation to frank adenocarcinoma, including abnormal glandular architecture, pleiomorphic nuclei and frequent mitotic figures (Fig. 2d–f). In addition, adenocarcinomas of the small bowel ($n = 2$) and colon ($n = 2$) were detected in this group of mice and all four tumours exhibited clear invasion of muscle (Fig. 2g). To determine the frequency of gastrointestinal pathology in the population, 10 mice from the G5–G7 $mTERC^{-/-}$ $p53^{+/-}$ cohort were killed and the caeca analysed (mean age 63 weeks). On gross examination, 6 out of 10 mice had either macroscopic polyps or thickened and irregular mucosa, and all 10 showed clear histological abnormalities including adenomatous hyperplasia and adenocarcinoma. Eleven $p53^{+/-}$ mice with intact telomeres ($mTERC^{+/+}$, $mTERC^{+/-}$ and G1–G2 $mTERC^{-/-}$) were analysed as controls

(mean age 50 weeks). The caeca from all 11 controls were normal on gross and histological examination. Despite the large size and invasiveness of these carcinomas, metastases were not detected.

To determine the mechanism by which telomere dysfunction accelerates tumour onset and shifts tumour spectrum, we analysed telomere maintenance and chromosomal structure in spontaneous cancers from $mTERC^{-/-}$ $p53$ mutant mice. Telomere PNA–fluorescent *in situ* hybridization (FISH) on metaphase spreads of lymphomas and breast cancers derived from late generation $mTERC^{-/-}$ mice revealed a high frequency of chromosome ends lacking telomere signal (signal-free ends) and numerous end-to-end fusions. In contrast, signal-free ends and fusions were uncommon in lymphomas from G1 $mTERC^{-/-}$ $p53^{-/-}$ mice (see Supplementary Information). Microscopic analysis revealed frequent anaphase bridges and lagging chromosomes in late generation $mTERC^{-/-}$ $p53^{+/-}$ breast carcinomas, but none in tumours arising in early generation $mTERC^{-/-}$ mice (see Supplementary Information). These bridges represent dicentric chromosomes pulled to opposite poles by the kinetochore/spindle apparatus leading to chromosomal breakage^{23,24}. Perhaps as evidence of increased breakage, small chromosomal fragments were detected in metaphase spreads of late generation $mTERC^{-/-}$ $p53$ mutant lymphomas and breast tumours, but not in G1 $mTERC^{-/-}$ $p53$ mutant lymphomas (Fig. 3d, arrows). Together, these data provide direct evidence for persistent telomere dysfunction in a subpopulation of tumour cells.

The availability of $p53$ null lymphomas from mice with normal telomeres and from mice with severe telomere dysfunction allowed us to study the impact of telomere dysfunction on chromosomal structure in the same tumour type. Spectral karyotyping (SKY)²⁵ revealed that $p53$ -null lymphomas with intact telomere function, including one $mTERC^{+/-}$ and one G1 $mTERC^{-/-}$ tumours, exhibited mild aneuploidy, but no fusions or translocations (Fig. 3a). These findings are consistent with studies^{26,27} indicating that the mechanism of $p53$ -deficient lymphomagenesis does not involve translocation to

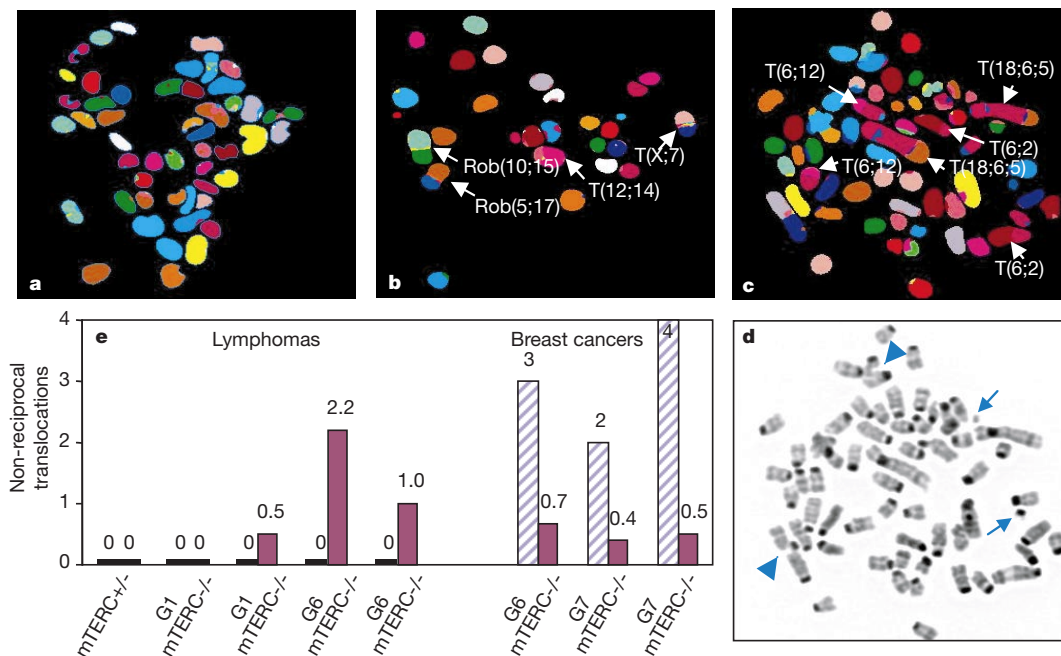


Figure 3 Spectral karyotyping. **a**, Metaphase spread, G1 $mTERC^{-/-}$ $p53^{+/-}$ lymphoma, showing no chromosomal rearrangements. **b**, G6 $mTERC^{-/-}$ $p53^{+/-}$ lymphoma, showing the presence of NRTs (T) and end-to-end chromosomal fusions (Rob). **c**, G7 $mTERC^{-/-}$ $p53^{+/-}$ breast carcinoma, showed aneuploidy and several complex NRTs, some of which involved multiple chromosomes. **d**, Reverse DAPI image of the same metaphase as in **c**

reveals marked genomic instability including chromatid breaks (arrowheads) and chromosome fragments (arrows). **e**, For each lymphoma and breast cancer analysed, the number of clonal NRTs (blue, striped) and non-clonal NRTs (pink) per metaphase is represented in a bar graph.

immunoglobulin gene loci. A second G1 mTERC^{-/-} p53^{-/-} lymphoma, originating 10 weeks later than the first, exhibited low numbers of end-to-end fusions—evidence for mild telomere dysfunction—and showed the emergence of interstitial chromosomal translocations of the non-reciprocal type. Notably, two G6 mTERC^{-/-} p53^{-/-} lymphomas exhibited numerous end-to-end fusions, indicating severe telomere dysfunction, and frequent non-reciprocal translocations (NRTs) (Fig. 3b, e). These data indicate that loss of telomere integrity due to progressive telomere shortening facilitates formation of NRTs.

In the lymphomas, both the end-to-end fusions and NRTs were non-recurrent; that is, consistent changes were not seen among multiple metaphases from the same tumour. SKY analysis of spontaneous breast tumours in G6 and G7 mTERC^{-/-} p53^{+/-} mice also revealed numerous complex NRTs and marked aneuploidy in all cases (Fig. 3c, d). In contrast to the lymphomas, each breast cancer exhibited recurrent NRTs, indicating a clonal origin of these rearrangements (Fig. 3e). In addition, non-recurrent NRTs were present at lower frequency in the breast cancer metaphases. These cytogenetics are remarkably similar to those of human breast cancers, which typically exhibit both clonal and non-clonal NRTs²⁸. Because breast cancers occurred in late generation mTERC^{-/-} p53^{+/-} mice only, tumours from transgenic models of mammary carcinoma were the best available controls to study chromosome structure in murine breast cancers with intact telomeres. Preliminary analysis of breast cancers from MMTV-Wnt-1 transgenic mice²⁹ revealed modest levels of aneuploidy and no NRTs (S.E.A. *et al.*, unpublished data). These results suggest that NRTs are not required for carcinogenesis in mouse mammary epithelial cells driven by a strong oncogenic stimulus.

Here we have shown that telomere dysfunction in p53 mutant mice promotes generation of NRTs, accelerates carcinogenesis and shifts the tumour spectrum toward one dominated by carcinomas. Non-reciprocal translocations have oncogenic potential in two ways: first, by carrying chimaeric or deregulated oncogenes at their breakpoints, as do reciprocal translocations; and second, by widely altering gene dosage. This latter process—the gain or loss of genetic information—makes NRTs fundamentally different from their balanced reciprocal counterparts. It is striking that human carcinoma cytogenetics are characterized by NRTs and that these rearrangements are often clonal within a tumour in similar fashion to the breast cancers that we describe here. In contrast to these adult tumours, NRTs are much less common in paediatric cancers such as lymphomas, leukemias and sarcomas, tumours in which reciprocal translocations frequently define the disease in molecular terms^{30,31}.

Propagation of a dicentric chromosome in plants has been shown to lead to structural gains and losses at the terminus of sister chromatids by repeated rounds of fusion-bridge breakage³². We propose that compromise of telomere integrity can lead to NRTs by a similar model of fusion-breakage translocation. Formation of dicentric chromosomes caused by telomere dysfunction may lead to chromosome breakage, generating recombinogenic free DNA ends that invade other chromosomes, yielding NRTs. Finally, the findings that telomere dysfunction generates these non-reciprocal changes and promotes carcinoma development provide a framework for understanding the well recognized but poorly understood paradox of episodic instability in human carcinomas. Telomere shortening in self-renewing compartments during life may compromise telomere function, leading to widespread gains and losses of chromosomal regions, and thus facilitating selection for an optimal genomic profile during tumour initiation. Further maturation is probably enhanced by quelling the extreme genomic instability of telomere dysfunction through telomerase reactivation. Our data suggest that ‘telonomic instability’ may initiate the neoplastic process and that telomerase reactivation may pave the transition to a more stable genome in which more subtle changes promote tumour progression. □

Methods

Mating scheme for generating mice

mTERC^{+/-} mice were mated with p53^{+/-} mice (Jackson Labs) to generate double heterozygotes (mTERC^{+/-} p53^{+/-}). Both strains are of mixed genetic background, primarily 129SV and C57Bl/6. These mice were intercrossed to generate G1 mTERC^{-/-} p53^{+/-} mice; G1 mTERC^{-/-} p53^{+/-} intercrosses yielded G2 mTERC^{-/-} p53^{+/-} mice and so on until G8. We used randomized cousin mating schemes to maintain genetic heterogeneity and prevent the generation of substrains¹⁷.

Tumour incidence and analysis

Mice were examined closely for evidence of ill health or overt tumour growth. Mice were killed if profoundly ill or if external tumours exceeded 2 cm in diameter and scored as a death in survival analysis. Only those animals with histologically proven cancer were scored as an event in the tumour incidence Kaplan–Meier analysis. Statistical significance was measured using the log-rank test. All mice were subjected to extensive autopsy and gross examination. Tumours were fixed in 10% formalin and embedded in paraffin. Five-µm paraffin sections were stained with haematoxylin and eosin.

Spectral karyotyping

Spectral karyotyping of lymphoma and breast cancer cell lines was done essentially as described²⁵. At least 12 metaphases were analysed for each of the breast carcinomas, and between 5 and 10 metaphases were analysed for each of the lymphomas. Structural aberrations were determined to be clonal if found in two or more metaphases.

Received 17 April; accepted 24 May 2000.

- Sedivy, J. M. Can ends justify the means?: telomeres and the mechanisms of replicative senescence and immortalization in mammalian cells. *Proc. Natl Acad. Sci. USA* **95**, 9078–9081 (1998).
- Harley, C. B., Futcher, A. B. & Greider, C. W. Telomeres shorten during ageing of human fibroblasts. *Nature* **345**, 458–460 (1990).
- Hastie, N. D. *et al.* Telomere reduction in human colorectal carcinoma and with ageing. *Nature* **346**, 866–868 (1990).
- Allsopp, R. C. *et al.* Telomere length predicts replicative capacity of human fibroblasts. *Proc. Natl Acad. Sci. USA* **89**, 10114–10118 (1992).
- Chadeneau, C., Hay, K., Hirte, H. W., Gallinger, S. & Bacchetti, S. Telomerase activity associated with acquisition of malignancy in human colorectal cancer. *Cancer Res.* **55**, 2533–2536 (1995).
- Kipling, D. & Cooke, H. J. Hypervariable ultra-long telomeres in mice. *Nature* **347**, 400–402 (1990).
- Prowse, K. R. & Greider, C. W. Developmental and tissue-specific regulation of mouse telomerase and telomere length. *Proc. Natl Acad. Sci. USA* **92**, 4818–4822 (1995).
- Broccoli, D., Godley, L. A., Donehower, L. A., Varmus, H. E. & de Lange, T. Telomerase activation in mouse mammary tumours: lack of detectable telomere shortening and evidence for regulation of telomerase RNA with cell proliferation. *Mol. Cell. Biol.* **16**, 3765–3772 (1996).
- Greenberg, R. A., Allsopp, R. C., Chin, L., Morin, G. B. & DePinho, R. A. Expression of mouse telomerase reverse transcriptase during development, differentiation and proliferation. *Oncogene* **16**, 1723–1730 (1998).
- Martin-Rivera, L., Herrera, E., Albar, J. & Blasco, M. A. Expression of mouse telomerase catalytic subunit in embryos and adult tissues. *Proc. Natl Acad. Sci. USA* **95**, 10471–10476 (1998).
- Nishizaki, T. *et al.* Genetic alterations in primary breast cancers and their metastases: direct comparison using modified comparative genomic hybridization. *Genes Chromosomes Cancer* **19**, 267–272 (1997).
- Buerger, H. *et al.* Comparative genomic hybridization of ductal carcinoma in situ of the breast—evidence of multiple genetic pathways. *J. Pathol.* **187**, 396–402 (1999).
- Al-Mulla, F., Keith, W. N., Pickford, I. R., Going, J. J. & Birnie, G. D. Comparative genomic hybridization analysis of primary colorectal carcinomas and their synchronous metastases. *Genes Chromosomes Cancer* **24**, 306–314 (1999).
- Kolquist, K. A. *et al.* Expression of TERT in early premalignant lesions and a subset of cells in normal tissues. *Nature Genet.* **19**, 182–186 (1998).
- Shpitz, B. *et al.* Telomerase activity in ductal carcinoma in situ of the breast. *Breast Cancer Res. Treat.* **58**, 65–69 (1999).
- Blasco, M. A. *et al.* Telomere shortening and tumour formation by mouse cells lacking telomerase RNA. *Cell* **91**, 25–34 (1997).
- Lee, H. W. *et al.* Essential role of mouse telomerase in highly proliferative organs. *Nature* **392**, 569–574 (1998).
- Hahn, W. C. *et al.* Creation of human tumour cells with defined genetic elements. *Nature* **400**, 464–468 (1999).
- Rudolph, K. L. *et al.* Longevity, stress response, and cancer in aging telomerase-deficient mice. *Cell* **96**, 701–712 (1999).
- Chin, L. *et al.* p53 deficiency rescues the adverse effects of telomere loss and cooperates with telomere dysfunction to accelerate carcinogenesis. *Cell* **97**, 527–538 (1999).
- Harvey, M. *et al.* Spontaneous and carcinogen-induced tumorigenesis in p53-deficient mice. *Nature Genet.* **5**, 225–229 (1993).
- Jacks, T. *et al.* Tumor spectrum analysis in p53-mutant mice. *Curr. Biol.* **4**, 1–7 (1994).
- Kirk, K. E., Harmon, B. P., Reichardt, I. K., Sedat, J. W. & Blackburn, E. H. Block in anaphase chromosome separation caused by a telomerase template mutation. *Science* **275**, 1478–1481 (1997).
- van Steensel, B., Smogorzewska, A. & de Lange, T. TRF2 protects human telomeres from end-to-end fusions. *Cell* **92**, 401–413 (1998).
- Liyanage, M. *et al.* Multicolour spectral karyotyping of mouse chromosomes. *Nature Genet.* **14**, 312–315 (1996).
- Nacht, M. & Jacks, T. V(D)J recombination is not required for the development of lymphoma in p53-deficient mice. *Cell Growth Differ.* **9**, 131–138 (1998).
- Liao, M. J. *et al.* No requirement for V(D)J recombination in p53-deficient thymic lymphoma. *Mol. Cell. Biol.* **18**, 3495–3501 (1998).
- Heim, S. & Mitelman, F. in *Cancer Cytogenetics* 369–388 (Wiley-Liss, New York, 1995).

29. Tsukamoto, A. S., Grosschedl, R., Guzman, R. C., Parslow, T. & Varmus, H. E. Expression of the int-1 gene in transgenic mice is associated with mammary gland hyperplasia and adenocarcinomas in male and female mice. *Cell* **55**, 619–625 (1988).
30. Atkin, N. B. Lack of reciprocal translocations in carcinomas. *Cancer Genet. Cytogenet.* **21**, 275–278 (1986).
31. Hilgenfeld, E., Padilla-Nash, H., Schrock, E. & Ried, T. Analysis of B-cell neoplasias by spectral karyotyping (SKY). *Curr. Top. Microbiol. Immunol.* **246**, 169–174 (1999).
32. McClintock, B. The stability of broken ends of chromosomes in *Zea mays*. *Genetics* **26**, 234–282 (1941).

Supplementary information is available on Nature's World-Wide Web site (<http://www.nature.com>) or as paper copy from the London editorial office of Nature.

Acknowledgements

We thank D. Castrillon for advice on tumour analysis; S. Ye for technical assistance; M. Novotny and C. Lam for technical assistance with histopathology; L. Rudolph, K. Wong, N. Sharpless, C. Khoo and N. Schreiber-Agus for critical reading of the manuscript. This work was supported by grants from the NIH to R.A.D. S.E.A. is a Howard Hughes Physician Postdoctoral Fellow and supported by a grant from the Massachusetts Department of Public Health. L.C. is a V foundation scholar and is supported by a NIH Mentored Clinician Scientist Award. R.A.D. is an American Cancer Society Professor. SKY analysis was performed in the Arthur and Rochelle Belfer Cancer Genomic Center at the Dana-Farber Cancer Institute.

Correspondence and requests for materials should be addressed to R.A.D. (e-mail: ron_depinho@dfci.harvard.edu).

Helix deformation is coupled to vectorial proton transport in the photocycle of bacteriorhodopsin

Antoine Royant^{††‡}, Karl Edman^{‡§}, Thomas Ursby^{*†}, Eva Pebay-Peyroula^{*}, Ehud M. Landau^{||} & Richard Neutze[‡]

* Institut de Biologie Structurale, CEA-CNRS-Université Joseph Fourier, UMR 5075, 41 rue Jules Horowitz, F-38027 Grenoble Cedex 1, France

† European Synchrotron Radiation Facility, 6 rue Jules Horowitz, BP 220, F-38043 Grenoble Cedex, France

‡ Department of Biochemistry, Uppsala University, Biomedical Centre, Box 576, S-751 23 Uppsala, Sweden

|| Biozentrum, University of Basel, Klingelbergstrasse 70, 4056 Basel, Switzerland

‡ These authors contributed equally to this work.

A wide variety of mechanisms are used to generate a proton-motive potential across cell membranes, a function lying at the heart of bioenergetics. Bacteriorhodopsin, the simplest known proton pump¹, provides a paradigm for understanding this process. Here we report, at 2.1 Å resolution, the structural changes in bacteriorhodopsin immediately preceding the primary proton transfer event in its photocycle. The early structural rearrangements² propagate from the protein's core towards the extracellular surface, disrupting the network of hydrogen-bonded water molecules that stabilizes helix C in the ground state. Concomitantly, a bend of this helix enables the negatively charged³ primary proton acceptor, Asp 85, to approach closer to the positively charged primary proton donor, the Schiff base. The primary proton transfer event would then neutralize these two groups, cancelling their electrostatic attraction and facilitating a relaxation of helix C to a less strained geometry. Reprotonation of the Schiff base by Asp 85 would thereby be impeded, ensuring vectorial proton transport. Structural rearrangements also occur near the protein's surface, aiding proton release to the extracellular medium.

Photoisomerisation of the bacteriorhodopsin (bR) chromophore from an all-*trans* retinal, covalently linked to Lys 216 through

a protonated Schiff base, to the 13-*cis* configuration is the initial event in the proton pumping mechanism. During its photocycle bacteriorhodopsin passes through a series of well characterized spectral intermediates, the simplest representation of which is $bR_{570} \rightarrow K_{590} \leftrightarrow L_{550} \leftrightarrow M_{412} \leftrightarrow N_{560} \leftrightarrow O_{640} \rightarrow bR_{570}$. The initial proton transfer occurs in the $L_{550} \rightarrow M_{412}$ transition. To elucidate the structural changes facilitating this transfer, we established conditions under which a high population of the low-temperature L intermediate (L_{LT}) builds up within crystals of wild-type bacteriorhodopsin grown in a lipidic cubic phase⁴, and determined the associated structural rearrangements.

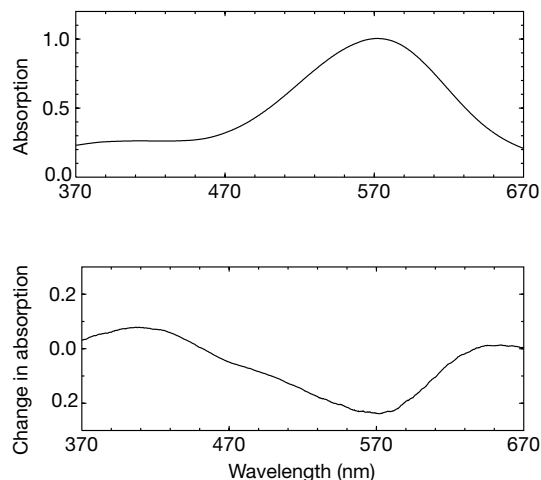


Figure 1 Spectral characterization of a bacteriorhodopsin (bR) intermediate trapped within a single crystal. **a**, Absorption spectrum of a typical light-adapted bR crystal in the ground state at 170 K. **b**, Difference spectrum between the spectrum of the crystal obtained 40 s after being illuminated for 30 s with green light ($\lambda = 532$ nm), and the spectrum shown in **a**. This spectrum is characteristic of a build up of the low-temperature L state (L_{LT}), with a small contribution from a deprotonated state.

Table 1 Diffraction data and refinement statistics

| Data set | Ground* | Excited |
|--------------------------------------|----------------------|----------------------|
| Resolution (Å) | 38–1.95 | 30–2.1 |
| No. of observations | 86,583 | 73,411 |
| No. of unique reflections | 16,826 | 13,088 |
| Completeness (%) (outer shell)† | 99.4 (99.1) | 96.6 (99.2) |
| R_{sym} (%)‡ (outer shell) | 4.1 (25.2) | 6.3 (52.1) |
| mean $I/\sigma(I)$ (outer shell) | 12.5 (2.9) | 9.0 (1.4) |
| Unit cell (Å) ³ | 60.84, 60.84, 110.49 | 60.96, 60.96, 109.97 |
| Twinning (%) | < 2 | 26 ± 2 |
| Conformers | | Ground/ L_{LT} |
| Occupancy (%) | | 30/70 |
| Number of atoms¶ | | |
| Total | | 1,798/1,776 |
| Protein | | 1,752/1,752 |
| Retinal | | 20/20 |
| Water | | 26/4 |
| R_{cryst} (%)# (outer shell)** | | 26.48 (29.35) |
| R_{free} (%)†† (outer shell) | | 28.82 (30.52) |
| r.m.s. deviation of bond lengths (Å) | | 0.0075 |
| r.m.s. deviation of bond angles (°) | | 1.15 |

* This corresponds to a new integration of the data that yielded the observations from which PDB entry 1qj1 was refined¹⁰.

† Outer shells were 2.06/1.95 and 2.21/2.10 Å for the ground state and the excited state, respectively. R_{merge} on the intensities between the ground state and the excited state corrected for twinning was 26.2%.

‡ $R_{sym} = \sum_i \sum_h |I_{h1} - \langle I \rangle| / \sum_i \sum_h I_{h1}$

§ The space group is $P6_3$.

|| The conformer corresponding to the Ground state was strictly fixed during refinement.

¶ Numbers correspond to the non-refined Ground state conformer and to the refined L_{LT} state conformer, respectively.

$R_{cryst} = \sum_h | |F_{obs}(h)| - |F_{calc}(h)| | / \sum_h |F_{obs}(h)|$

** Refinement outer shell was 2.17/2.10 Å.

†† Calculated from a set of 5% randomly selected reflections that were excluded from refinement. This set of reflections is identical to the one used in the ground state refinement. The R_{free} for the ground state refinement was 24.5%.